Determination of Electron Transfer Kinetic Parameters by Fourier Transform Electrochemical Impedance Spectroscopic Analysis

Byoung-Yong Chang, Sung-Young Hong, Jung-Suk Yoo, and Su-Moon Park*

Department of Chemistry and Center for Integrated Molecular Systems, Pohang University of Science and Technology, Pohang, Gyeongbuk 790-784, Korea

Received: March 22, 2006; In Final Form: May 30, 2006

A new attempt to obtain electron transfer kinetic parameters at an electrified electrode/electrolyte interface using Fourier transform electrochemical impedance spectroscopic (FTEIS) analyses of small potential step chronoamperometric currents is presented. The kinetic parameters thus obtained allowed mass transport free voltammograms to be constructed in an overpotential region, where the diffusion limits the electron transfer reaction, using the Butler−Volmer (B−V) relation. The B−V voltammograms clearly distinguish electrode reactions that are not much different in their electron transfer kinetic parameters, thus showing very similar normal linear sweep voltammetric (SCV) behaviors. Electrochemical reduction of *p*-benzoquinone, which displays nearly the same SCV responses at a gold electrode regardless whether the electrode is covered by a thiolated β-cyclodextrin self-assembled monolayer, was taken as an example for the demonstration. The results show that the two voltametrically similar systems display very different electron transfer characteristics.

Introduction

Traditionally, voltammograms, in which currents are plotted as a function of applied potential, have been used to describe an electrode reaction at the electrode/electrolyte interface, because the currents are a measure of the electrode reaction kinetics for its activational parameter, overpotential.[1] The current has two components, Faradaic and non-Faradaic, of which the non-Faradaic component is not related to the electrode reaction and is often regarded as noise. Investigators have been trying to minimize the non-Faradaic component as much as possible; the normal-pulse and differential-pulse modes of voltammetric or polarographic experiments have evolved from dc polarography and linear sweep voltammetry.[2] Recently, almost complete removal of capacitive contributions has been achieved using programmed potential voltammetry, which enhances the sensitivity by orders of magnitude.[3] While the minimization of noise would certainly bypass the problem to a certain extent, a better approach would be to measure both components concurrently and have a full description of the system using the information thus obtained.[4]

The Faradaic current is determined by two major parameters, an activation barrier for the electron transfer and the transport of the electroactive material toward the electrode surface, along with other parameters such as solution resistance, transfer coefficients, and so forth, affecting to lesser extents.[5] The electron transfer kinetics has been described in the form of the Butler−Volmer (B−V) equation; also, the mass transport effects had to be taken into account for a full description of the overall currents in electrochemical reactions. The B−V kinetics taking into account only the activational parameters (overpotential, η, and transfer coefficient, α) without considering the effect of mass transport has an expression

$$i = i^0\left[\exp\left(\frac{-\alpha nF}{RT}\eta\right) - \exp\left(\frac{(1-\alpha)nF}{RT}\eta\right)\right] \qquad (1)$$

where i^0 is the exchange current, n the number of electrons transferred, F the Faraday constant, R the gas constant, and T the absolute temperature. The voltammetric currents can be approximated by the B−V equation when η is small by ignoring the effect of mass transfer, but the latter starts to limit the current as η becomes larger.[5] To separate these two effects, electrochemists have been making measurements by modulating either the rate of mass transport or the electron transport. Examples include voltammetric measurements at rotating disk electrodes (RDEs) and/or at ultramicroelectrodes (UMEs), variation of scan rates in linear sweep voltammetric experiments, and modulation of electron transfer characteristics by modifying electrode surfaces with, e.g., a self-assembled monolayer (SAM).[6] At RDEs and UMEs, the range of the overpotential, at which the mass transport starts to limit the electron transfer, can be extended due to more effective mass transport.[1] The overpotential range is also extended by slowing down the rate of electron transfer at the modified electrode surface.[6] This is because the B−V expression had to be used for the estimation of the rate constant in a relatively narrow overpotential region where the mass transport effect is significant. When η becomes large enough to make the electron transfer faster in comparison to that of mass transfer, the current expression does not contain an electron transfer parameter any more as in the Cottrell equation.[5] However, the mass transport effect is still present even when η is small,[7] although its contribution is usually ignored in the data treatment.

While the electrokinetic parameters can be obtained from the experiments mentioned above, impedance measurements offer a better way to describe the interface.[2,4] With the information on the impedances at the electrode−electrolyte interface, we can not only separate Faradaic from non-Faradaic components but also distinguish the charge transfer resistance from the mass

* E-mail: smpark@postech.edu; phone: +82-54-279-2102; fax: +82-54-279-3399.

10.1021/jp061773y CCC: $33.50
Published on Web 09/02/2006

transport impedance. Impedance measurements have been made by applying a small ac voltage at a wide range of frequencies. Problems involved in this method of impedance measurements include (1) too much time taken to make real-time measurements, as the measurements are made when a steady state is reached,[3] and (2) a large contribution of the Warburg impedance when the rate of electron transfer is relatively large, making it difficult to extract the electrokinetic parameters. Difficulties and questions as to the validity of impedance data obtained at steady states have been raised by many investigators.[8−10] Recently, we have thus developed a Fourier transform electrochemical impedance spectroscopic (FTEIS) technique, which allows real-time snapshots of impedance to be taken at any overpotential; details have been described elsewhere.[11]

In this work, we demonstrate that the two electrochemical systems showing essentially the same voltammetric responses can be quite different when presented in a different format of electrokinetic expression. To show how a subtle difference in electrode kinetics may be magnified, we chose *p*-benzoquinone (*p*-BQ) reduction at bare and thiolated β-cyclodextrin (β-CD) self-assembled monolayer (SAM)-covered gold electrodes, at which cyclic voltammetric (CV) responses are almost indistinguishable.[12] The β-CD SAM-covered electrode is regarded as an array of nanoelectrodes with their surfaces exposed to the solution through cavities of β-CD,[12b] at which essentially the same voltammogram as that at the same electrode without the SAM is obtained due to the overlap of their diffusion layers. We demonstrate that the voltammograms represent only part of an electrochemical system, while the results of impedance measurements lead to a full description of the system.

Experimental Section

A homemade, fast-rise potentiostat was the main device for the impedance measurements.[12a] An Agilent 33120 arbitrary waveform generator was connected to the potentiostat as a high-speed step function generator and a PC was connected to it via a PCI interface card with a Gage Compuscope 1610 high-speed data acquisition system as was described elsewhere.[11b] The electrochemical cell had three electrodes, gold disk working (area = 0.025 cm^2), larger platinum gauge counter, and Ag/AgCl (in saturated KCl) reference electrodes. The working electrode was either bare or covered with the mixed SAM of thiolated β-CD and *n*-pentanethiol; preparation of the β-CD covered electrode has been described elsewhere.[12a] The open space between immobilized β-CD molecules was sealed with small amounts of *n*-pentanethiol, and thus, it is regarded as a nanoelectrode array.

For the electrochemical measurements, an aqueous solution of 0.12 mM *p*-BQ and 0.20 M $Na_2SO_4$was used. The staircase voltammetry experiments were conducted by applying a series of increasing potential steps.[11b,13] Each potential step of 7.5 mV was applied to the working electrode at every 25 ms in a potential range of 0.2 to −0.4 V; this corresponds to 300 mV/s of a scan rate for the voltammetric experiment. The current was sampled at a rate of 200 k samples/s after the application of each potential step.

For every 25 ms potential step, both the potential and current data acquired were used for the calculation of impedance data. Staircase cyclic voltammograms (SCVs) were obtained with averaged currents of the last 10 ms of each data segment. Impedances were computed from chronoamperometric currents recorded for 25 ms after each step by first taking the first derivatives of the step voltage and the resulting currents,[7,11] followed by fast Fourier transform (FFT) with frequencies ranging from $1/t_{total}$ (lower limit) to $1/(2\Delta t)/30$ (upper limit). The upper limit of the frequency would be $1/(2\Delta t)$, but it was set at $1/(2\Delta t)/30$ because the currents at frequencies higher than $1/(2\Delta t)/30$ were found to contain a significant amount of noise. Here, Δt is the sampling interval, and t_{total} is simply the sampling period, $N\cdot\Delta t$, with N being the total number of samples. The FFT calculations were carried out using the *Matlab* program (MathWorks, Natick, MA), and circuit simulations were conducted to fit the observed values to the proposed equivalent circuits using the *ZSimpWin* program of EG&G.

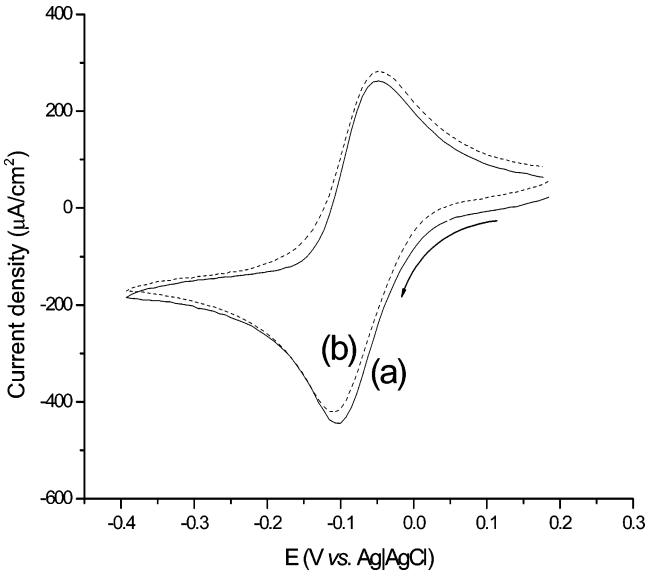

Figure 1. SCVs of (a) *p*-BQ on the bare gold electrode (—) and (b) *p*-BQ on the mixed-SAM-covered gold electrode (- - -).

Results and Discussion

Figure 1 shows typical staircase cyclic voltammograms (SCVs) obtained from *p*-BQ reduction at bare (a; —) and mixed-SAM-covered (b, - - -) gold electrodes. The two SCVs for *p*-BQ reduction at bare and SAM-modified electrodes are very similar to cyclic voltammograms (CVs) obtained under the same experimental conditions.[12,13] The SCVs show that *p*-BQ undergoes a reversible, one-electron transfer reaction to produce its anion radical as a product with a peak separation of about 60 mV.[14] The two voltammograms appear practically indistinguishable except that the peak potential is shifted in a slightly negative direction at the SAM-covered electrode, indicating that its electrode kinetics should be slightly slower than that at the bare electrode. While gold surfaces covered by ω-hydroxythiol of different carbon chain lengths modulated the rate of electron transfer to a great extent,[6] the thiolated β-CD-covered electrode does not appear to.

It is well-established that essentially the same voltammograms are observed at bare and microarray electrodes when the diffusion layers of each microelectrode overlap with each other.[12b,c] Here, the β-CD cavities act as a nanoelectrode array where the interelectrode distance is much smaller in relation to the diffusion-layer thickness.[12b] The similarity of the two voltammograms indicates that the diffusion component overwhelms the current, and thus, the electron transfer kinetics does not make differences in determining the shapes and currents of the SCVs under the conditions used.[6,15]

To see the difference in kinetic characteristics of the two systems, we transformed the chronoamperometric currents obtained upon application of a series of small potential steps to impedance data using the FTEIS procedure.[11] Figure 2 shows

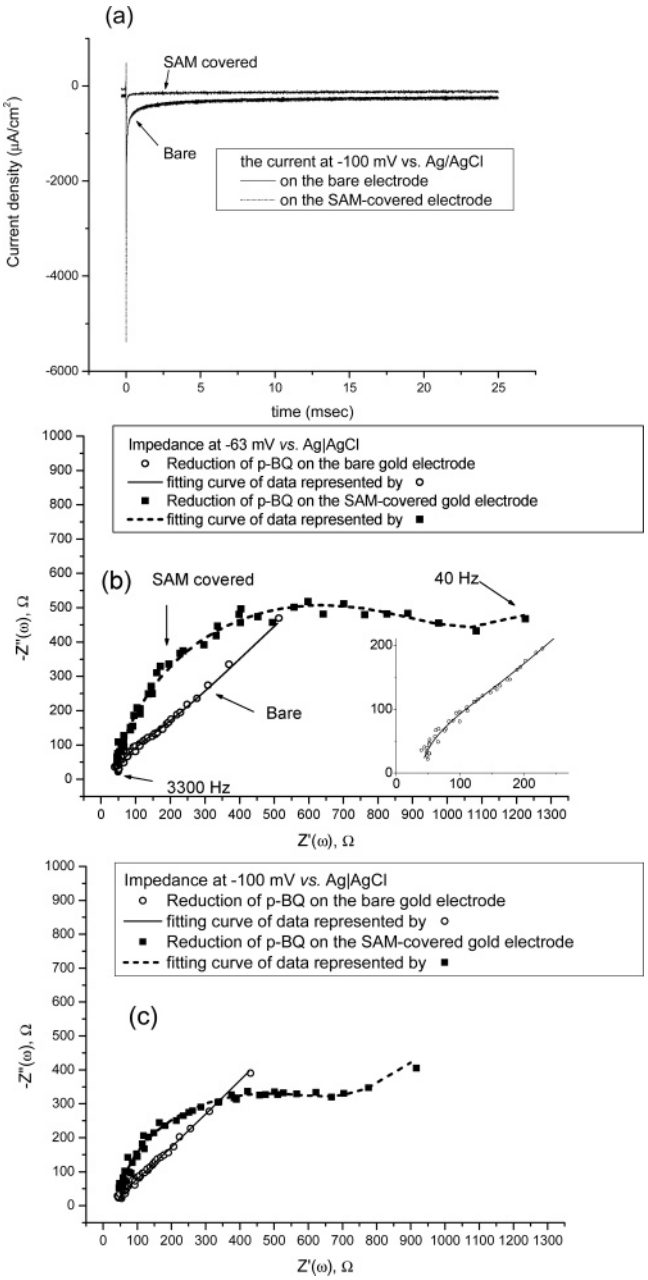

Figure 2. (a) Chronoamperometric currents obtained upon applying a potential step of 7.5 mV at the dc bias potential at −100 mV at the bare (—) and SAM-covered (- - -) electrodes; (b) Nyquist plots of impedance on the imaginary plane, $-Z''(\omega)$, vs impedance on the real plane, $Z'(\omega)$, for reduction of *p*-BQ at the bare (-○-) and mixed-SAM-covered (-■-) electrodes at −63 mV and (c) at −100 mV. An expanded version of impedance plots at the bare electrode is shown in (b) as an inset. Symbols represent the experimental data, and lines represent fitting curves using equivalent circuits shown in Figure 3. Note that the baseline for the current at the bare electrode was slightly lifted for a better inspection of the two curves. The frequency range for the impedance plots shown in (b,c) was 3300 and 40 Hz.

(a) typical chronoamperometric current curves obtained at −0.10 V for *p*-BQ reduction at bare (solid line) and SAM-covered (dashed line) electrodes, (b) the Nyquist plots of the impedances at −63 mV, and (c) the plots converted from the data shown in (a). The equivalent circuits shown in Figure 3 were found to provide the best fits for all the impedance data obtained at bare (a) and the SAM-covered (b) electrodes in a wide range of the bias potential. Figure 2 shows that the Nyquist plots shown for *p*-BQ reduction at the SAM-covered electrode (-■-) are significantly depressed, while those at the bare electrode (-○-)

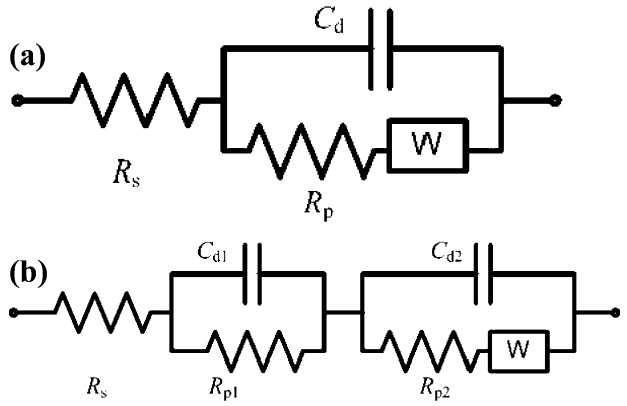

Figure 3. Equivalent circuits used for simulating impedance plots shown for *p*-BQ reduction on the bare (above) and mixed-SAM-covered (below) electrodes. Here, R_s, R_p, C_d, and W represent the solution resistance, polarization resistance, double-layer capacitance, and Warburg impedances, respectively.

are dominated by the Warburg (mass transport) impedance, as can be seen from a 45° Warburg line in the plot. The depressed semicircles are observed when more than one electrochemical processes are convoluted, as shown in Figure 3b, or when a constant phase element (CPE) replaces the capacitor even in the equivalent circuit shown in Figure 3a due to a highly porous electrode surface.[16] Of the two possibilities considered for fitting the impedance data shown in Figure 2b,c, the circuit with two electron transfer processes shown in Figure 3b gave better fittings than the one with C_d replaced by a CPE in Figure 3a.

It is noted in Figure 2b,c that almost indistinguishable SCVs and chronoamperometric current responses (Figures 1 and 2a) show entirely different behaviors when they are converted to the impedance data. A few points can be made about the results. First, there is only one electrochemical reaction involved in *p*-BQ reduction at the bare electrode, while two processes are involved in the SAM-covered electrode as indicated by two $R_p{\cdot}C_d$ loops representing two semicircles; here, R_p is a polarization resistance (vide infra), and C_d is the double-layer capacitance. The presence of two $R_p{\cdot}C_d$ semicircles indicates that two electrochemical processes having different *RC* time constants are convoluted to give a single current transient shown in Figure 2a (dashed line); that is, two reactions with two different *RC* time constants, $R_{p1}{\cdot}C_{d1}$ for the first semicircle at higher frequencies and $R_{p2}{\cdot}C_{d2}$ for the second at lower frequencies, occur in series. Second, the rate of electron transfer is much higher at the bare electrode, as indicated by smaller diameters of the semicircles, which represent the polarization resistances at the applied bias potentials,[4a] in comparison to that at the SAM-covered electrode. The polarization resistance is defined as $d\eta/di$ from eq 1 at a given η value.[4] Moreover, the impedance for *p*-BQ reduction at the bare electrode is completely overwhelmed by the Warburg component, because the rate of electron transfer is high enough to be limited by the rate of mass transport even at high frequencies. Here, we reserve the term the charge-transfer resistance (R_{ct}), as it is defined as the resistance to charge transfer at $\eta = 0$; the resistance to charge transfer at any other overpotentials should be termed the polarization resistance (R_p). The R_ps are much greater at the SAM-covered electrode than those at the bare electrode, as would be readily expected. Thus, the impedance analyses of what appeared to be the two very similar CVs and current decays, as shown in Figures 1 and 2a, display significantly different reaction kinetics.

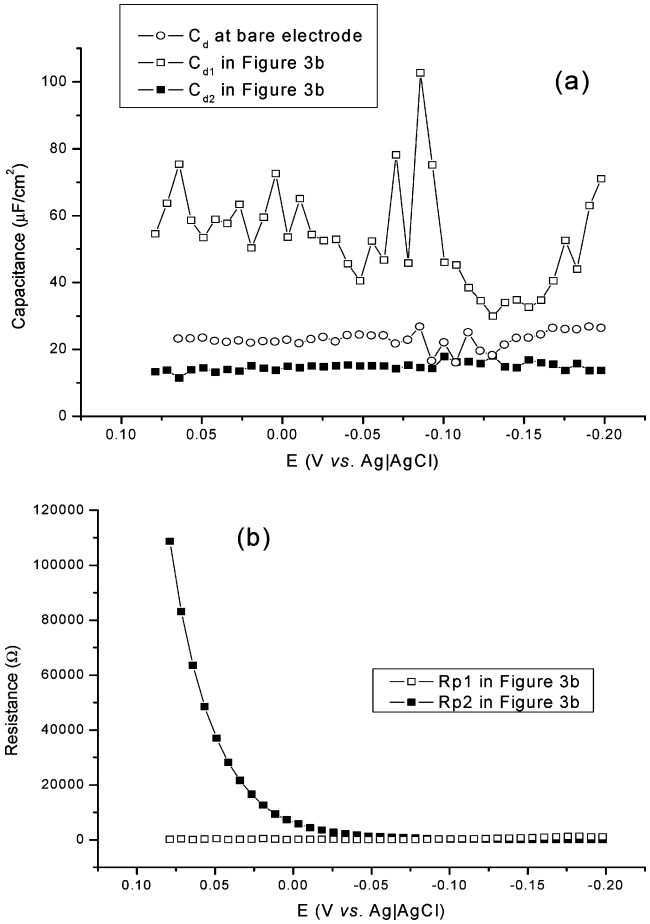

Figure 4. (a) Double-layer capacitances obtained from the semicircles in the higher (-□-) and lower (-■-) frequency regions for the SAM-covered and bare (-○-) electrodes and (b) polarization resistances obtained from the higher- (-□-) and lower- (-■-) frequency *RC* loops. Here, the higher-frequency semicircle indicates the one on the left in Figure 3b, while the one on the right is a process occurring at lower frequencies. Note that these two are naturally convoluted.

The results of the impedance analysis for *p*-BQ reduction using the equivalent circuits in Figure 3 are shown in Figure 4. As described above, the circuit shown in Figure 3a was used to fit the impedance data obtained at the bare electrode, while the one in Figure 3b was used for the SAM-covered electrode. We see from Figure 4a that the capacitances obtained from the first *RC* loop (-□-) at the SAM-covered electrode are significantly larger than those from the second semicircle (-■-) as well as from the bare electrode (-○-). Also, Figure 4b shows that R_{p1}s for the first charge transfer (-□-) are nearly independent of the overpotential in a wide range of potentials and much smaller than those for the second semicircle (-■-) except at high overpotentials. These observations suggest that the reaction characterized by a time constant, $R_{p1}\cdot C_{d1}$, in the high-frequency region is similar to underpotential (UPD) reduction of *p*-BQ in its behavior. The R_ps for UPD deposition of metal ions are nearly independent of the potential applied, and the capacitances involved in the reaction were shown to be significantly larger than those for the normal overpotential reactions.[17] This is because the UPD is not a potential-activated process, which is due to the affinities of the deposited metal to the substrate electrode. We note, however, that these R_{p1}s gradually increase upon increase in overpotentials on the SAM-covered electrode (Figure 4b, □), which is attributed to the difficulty in getting *p*-BQ molecules through the β-CD cavity and getting the reduced *p*-BQ (anion radical) out of the cavities, when all the

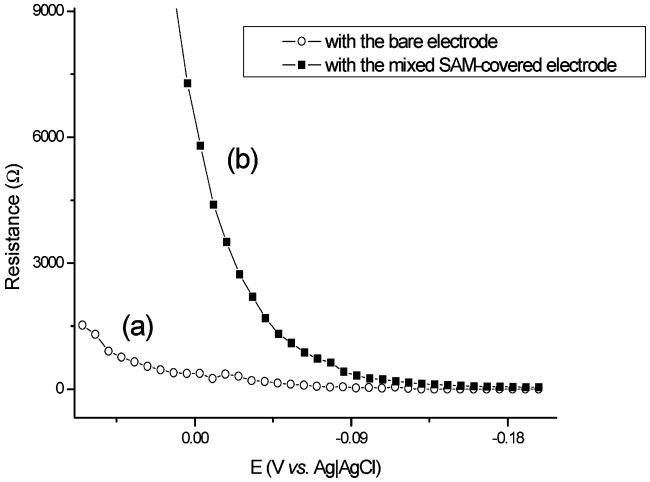

Figure 5. Comparisons of R_p values for *p*-BQ reduction at bare (a) and mixed-SAM-covered (b) electrodes. The data shown in (b) are the same as that shown in Figure 4b (-■-).

p-BQ molecules inside the cavity have been reduced. These behaviors are consistent with a picture in which the first semicircle represents reduction of *p*-BQ molecules captured inside the β-CD cavities;[12a] in other words, the *p*-BQ molecules behave like adsorbed molecules inside the β-CD cavities, and its reduction does not require much activation energy as a regular overpotential-activated electrochemical process would. Further, the excess anions electrogenerated from the reduction of *p*-BQ are confined inside cavities at the molecular scale forming a large double-layer capacitor with cations above the cavities; the point of zero charge is about 0.2 V in the 0.02 M Na_2SO_4 solution[18] and the electrode surface, which must already be negatively charged, would be even more strongly charged with negative ions in the potential region, making them even larger capacitors. The fluctuations in capacitances when the *p*-BQ molecules begin to be reduced are also explained by the excess anion radicals that *p*-BQ generated, which would upset the ion balance leading to the fluctuations. These fluctuations are observed at both the SAM-covered (-□-) and bare (-○-) electrodes as shown in Figure 4a, although they are not as large at the bare electrode for an obvious reason. Note, however, that the reaction represented by the second semicircle with time constants $R_{p2}\cdot C_{d2}$ in the lower-frequency region shows typical characteristics of electron transfer across a somewhat passivated surface with small but almost constant capacitances (-■-, Figure 4a) when the overpotential increases to large values. The polarization resistance decays exponentially along with the increasing overpotential (Figure 4b, -■-) until to a certain value but then slightly increases upon further increase in overpotential beyond about −0.1 V; this is a behavior expected from a passivated surface. This is because the electron transfer would take place across the SAM-covered surface via tunneling[6] and/or through the reduced *p*-BQ inside β-CD cavities acting as mediators. Due to the hydrophobic nature of organic molecules covering the electrode, the SAM-covered electrode would show smaller capacitances than the bare one.

Figure 5 shows the comparison of the R_ps obtained at bare (a) and SAM-covered (b) electrodes. As already pointed out, the R_p values at the SAM-covered electrode are in general much greater than those at the bare electrode; both of them decrease exponentially as a function of the increasing overpotential. Here, we use the R_ps obtained from the second semicircle in the lower-frequency region for the SAM-covered electrode, because the first semicircle at higher frequencies is apparently not the

overpotential-activated process as already discussed. Because the charge transfer reaction is significantly faster at the bare electrode as can be seen from significantly smaller R_p values in comparison to those at the SAM-covered electrode, the mass transport limits the reaction at higher frequencies, which is why the Warburg line overwhelms the small semicircle even from rather high frequencies (Figure 2b,c, -○-). On the other hand, it is clearly seen from Figure 2b,c that the contribution from the Warburg impedance is beginning to become increasingly important at the SAM-covered electrode as the overpotential is increased from −63 mV to −100 mV (lines represented by -■-). In other words, the Warburg line starts to intercept the semicircle from a smaller diameter at −100 V than at −63 mV. Here, the overpotential-activated process controls the overall reaction rate rather than the mass transport does until the overpotential becomes large enough for the mass transfer to limit the overall process. Nevertheless, the currents obtained by averaging those sampled between 15 and 25 ms are nearly the same at both bare and SAM-covered electrodes, giving almost the same SCVs, because the mass-transport-dominated currents are read by the time the currents are sampled. This explains the two very similar SCVs, although the R_p values are significantly different.

When the mass transport effect is either removed or not important enough, the current should follow the B−V kinetics, eq 1.[5] The equation predicts that the R_p, defined as $d\eta/di$, would be decreasing exponentially as the overpotential increases, in excellent agreement with those shown in Figure 5. In a recent study, Jurczakowski and Lasia[19] reported from their computer-aided computation of the impedance data that the R_p value goes through a minimum at the standard reduction potential, $E°$, for a reversible electrochemical system. This is because they used a current expression for the potential step

$$i_f = nFA(k_f \cdot C_O^* - k_b \cdot C_R^*) \cdot \exp(H^2 t) \cdot \mathrm{erfc}(Ht^{1/2}) \qquad (2)$$

for their calculation. Here, $H = k_f/\sqrt{D_O} + k_b/\sqrt{D_R}$, where D_O and D_R are diffusion coefficients of the oxidant and reductant, C_O^* and C_R^* are bulk concentrations, A is the electrode area, and k_f and k_b are forward and backward reaction rate constants for the electron transfer reaction

$$\mathrm{Ox} + \mathrm{e} \underset{k_b}{\overset{k_f}{\rightleftharpoons}} \mathrm{Red} \qquad (3)$$

Equation 2 has been derived on the basis of assumptions that the system is in equilibrium, both the oxidant and the reductant are initially present, and the rate of the electrochemical reaction, i_f, is determined by both the activation parameters (k_f and k_b in eq 2) as well as the diffusion parameters (H in the same equation).[20] When the diffusion, or the mass transport, is factored in, it is readily expected that the R_p value would show a minimum at $E°$, where no mass transport plays a role and only an exchange current flows when the concentrations of the oxidant and the reductant are the same. The mass transport would present impedances (or resistances) to the overall charge transfer on both sides of $E°$, making them larger than that at $E°$. In our case, however, we have obtained the R_p values for only the overpotential-activated process with the mass transport effect completely removed from consideration, which represent true R_ps that would be obtained from eq 1. Note that no mass transport has been considered in the B−V expression of the current as seen from eq 1.

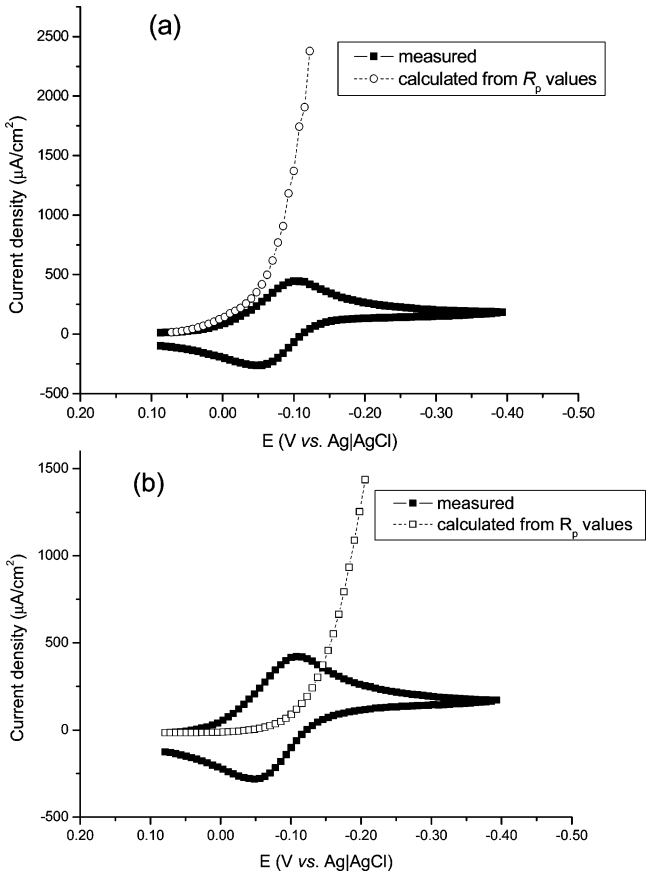

Figure 6. Mass transport free currents calculated from R_p values along with SCVs at bare (a) and SAM-covered (b) electrodes.

Employing the R_p values, one can evaluate the overpotential-activated, virtual current from the impedance data using an equation

$$i = \int \frac{1}{R_p} d\eta \qquad (4)$$

which is simply an integrated form of the definition of the polarization resistance[4]

$$R_p = d\eta/di \qquad (5)$$

For this calculation, the overpotentials were taken as the difference between the potential applied and $E°'$, which was estimated by taking an average of cathodic and anodic peak potential of the reversible SCVs shown in Figure 1. The "mass transport free" voltammograms thus obtained are shown in Figure 6 for the bare and SAM-covered electrodes along with the SCVs. One can see from Figure 6 (-○- in (a) and -□- in (b)) that the increase in current follows the exponential relation given by the B−V kinetics (eq 1) if the mass transport does not limit the currents at high overpotentials. By nonlinear fitting of the data to the B−V equation and also from the Tafel equation (plots not shown), electron transfer rate constants, k^0, and transfer coefficients, α, were determined to be 1.6×10^{-3} and 1.1×10^{-4} cm/s and 0.64 and 0.59, respectively, at bare and SAM-covered electrodes. The exchange rate constant for *p*-BQ is in good agreement with the one reported in the literature (9.7×10^{-4} cm/s and $\alpha = 0.79$) under similar experimental conditions.[21] The mass transport free currents at the bare electrode are much higher than the SCV currents at higher overpotentials, which would have been the current predicted by the B−V relation, had it not been limited by the mass

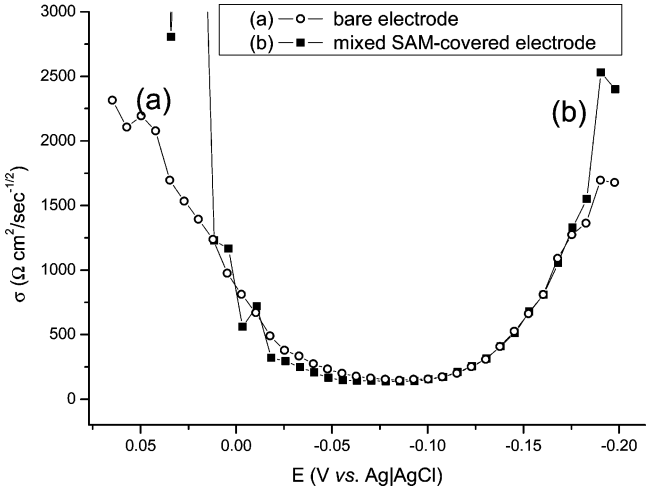

Figure 7. The σ-values obtained from the impedance data at bare (a) and SAM-covered (b) electrodes. The impedance data used here were obtained from chronoaperometric currents obtained throughout the whole potential region. Two examples at two potentials are shown in Figure 2b,c.

transport. On the other hand, the mass transport free currents are smaller than the SCV currents at the SAM-covered electrode (Figure 6b) until the overpotential becomes very high, indicating that the average diffusion currents sampled between 15 and 25 ms are greater than those obtained from the overpotential activated process. More will be discussed on this below. Under an appropriate experimental condition, one can extend the potential range of the measurements of polarization resistance deep into the diffusion-limited region, and the enhancement in current could be as high as a few hundred times the diffusion-limited current.[4]

The effects of mass transport have been evaluated from the data shown in Figure 2b,c by obtaining the σ-values having the following expression[2]

$$\sigma = \frac{RT}{\sqrt{2}F^2A}\left(\frac{1}{\sqrt{D_{ox}}\cdot C^*_{ox}} + \frac{1}{\sqrt{D_{red}}\cdot C^*_{red}}\right) \qquad (6)$$

at various overpotentials, and the results are shown in Figure 7. The evaluation of the σ values is possible because the current, $i(t)$, obtained at time t, upon stepping a potential, ΔV, for the equivalent circuit shown in Figure 3a contains the σ term as can be seen from the following expression for an electrochemical cell represented by equivalent circuits shown in Figure 3[7]

$$i(t) - i(t \le 0) = \frac{-\Delta V}{R_p + R_s}\cdot\exp\left[\left(\frac{\sqrt{2}\sigma}{R_p + R_s}\right)^2\cdot t\right]\cdot \mathrm{erfc}\left[\frac{\sqrt{2}\sigma}{R_p + R_s}\cdot\sqrt{t}\right] + \frac{-\Delta V\cdot R_p}{R_s(R_p + R_s)}\cdot\exp\left[-\frac{(R_p+R_s)t}{R_pR_sC_d}\right] \qquad (7)$$

Here, $i(t \le 0)$ is the current that might have been flowing before the potential step. The impedance analysis gives σ values, the effect of mass transfer. Although σ should be independent of potential according to eq 6, the variations in σ values in Figure 7 indicate that C^*_{ox} and C^*_{red} should have been $C_{ox}(x = 0)$ and $C_{red}(x = 0)$ in eq 6 instead, where x is the distance from the electrode surface; in other words, the surface concentrations should be used in the expression.[2] The minimum σ value is then observed at $E°$, where $C_{ox}(x = 0)$ should be close to $C_{red}(x = 0)$. At higher or lower overpotentials, either $C_{ox}(x = 0)$ or $C_{red}(x = 0)$ becomes close to 0, resulting in larger σ values. In the intermediate potential region, the ratio of $C_{ox}(x = 0)$ to $C_{red}(x = 0)$ would be determined by the Nernst equation, leading to slowly changing σ values between -25 and -125 mV as shown in Figure 7.

As a final point, we realize that the SCV current is significantly higher than the overpotential-activated current at the SAM-covered electrode at overpotentials smaller than about -120 mV (Figure 6b). This is because the currents sampled at $t \ge 15$ ms are mainly from large fluxes of electroactive species effectively diffusing toward the UMEs after the transient currents decay. This is why the voltammetric current observed on a microelectrode array has the same shape and magnitude as that at a disk electrode of the same total area of the array electrodes with the insulating spaces between where their diffusion layers overlap with each other. However, important information is contained in the current transient at shorter sampling periods (higher frequencies), as we have demonstrated here.

Conclusions

In this work, we have demonstrated that what appear to be almost the same electrochemical reactions when viewed by traditional voltammetric signals[12] can be resolved into the reactions of entirely different characteristics by performing a full FTEIS analysis of the chronoamperometric current obtained upon application of a small voltage step signal. The analysis provides detailed information as to the electrode kinetics of the reaction, and the information thus obtained allows the electrode−electrolyte interface to be fully described. All this information was obtained during a single scan corresponding to a single cyclic voltammetric recording, ~4 s, which of course was followed by signal analyses.

As an example for this analysis and interpretation thereof, we took *p*-BQ reduction at bare and SAM-covered electrodes, which display almost identical SCV and CV responses, and demonstrated that the reaction showed entirely different behaviors when presented in a different format, i.e., the mass transport free voltammograms. It was found also that the *p*-BQ reduction at the mixed-SAM-covered electrode proceeds via two consecutive processes: one overpotential-independent and the other overpotential-activated.

Our work is expected to have a few significant impacts on electrochemical measurements and their interpretation in that the transient currents are fully taken advantage of for extraction of useful information. The earlier transients have usually been discarded thus far in traditional electrochemical experiments.[5] The technique should also offer high-throughput recordings of impedance signals for studying interactions and analysis of biologically important compounds.[21] Finally, the technique should allow the time-resolved electrochemistry to be conducted when the technology advances enough to analyze the transient at very high frequencies.

Acknowledgment. This research was supported by the grant from the KOSEF through the Center for Integrated Molecular Systems located at Postech. The authors are also grateful for graduate stipends provided to B.Y.C. by the BK-21 program of the KRF.

References and Notes

(1) See, for example, Bard, A. J.; Faulkner, L. R. *Electrochemical Methods*; John Wiley and Sons: New York, 2001; Chapter 6.

(2) See Chapter 13 of ref 1.

(3) Yoo, J.-S.; Park, S.-M. *Anal. Chem.* **2005**, *77*, 3694.

(4) (a) Park, S.-M.; Yoo, J.-S. *Anal. Chem.* **2003**, *75*, 455A. (b) Park, S.-M.; Yoo, J.-S.; Chang, B.-Y.; Ahn, E.-S. *Pure Appl. Chem.* **2006**, *78*, 1069.

(5) See Chapters 3−5 of ref 1.

(6) (a) Miller, C.; Cuendet, P.; Grätzel, M. *J. Phys. Chem.* **1991**, *95*, 877. (b) Miller, C.; Grätzel, M. *J. Phys. Chem.* **1991**, *95*, 5225. (c) Becka, A. M.; Miller, C. J. *J. Phys. Chem.* **1992**, *96*, 2657.

(7) Chang, B.-Y.; Park, S.-M. *Anal. Chem.* **2006**, *78*, 1052.

(8) (a) Sluyters-Rehbach, M.; Sluyters, J. H. *J. Electroanal. Chem.* **1979**, *102*, 415. (b) Popkirov, G. S.; Schneider, R. N. *Electrochim. Acta* **1993**, *38*, 861.

(9) (a) Stoynov, Z. B.; Savova-Stoynov, B. S. *J. Electroanal. Chem.* **1985**, *183*, 133. (b) Savova-Stoynov, B.; Stoynov, Z. B. *Electrochim. Acta* **1992**, *37*, 2353. (c) Stoynov, Z. *Electrochim. Acta* **1992**, *37*, 2357. (d) Stoynov, Z. *Electrochim. Acta* **1993**, *38*, 1919.

(10) Urquidi-Macdonald, M.; Real, S.; Macdonald, D. D. *Electrochim. Acta* **1990**, *35*, 1559.

(11) (a) Yoo, J.-S.; Park, S.-M. *Anal. Chem.* **2000**, *72*, 2035. (b) Yoo, J.-S.; Song, I.; Lee, J.-H.; Park, S.-M. *Anal. Chem.* **2003**, *75*, 2962.

(12) (a) Lee, J.-Y.; Park, S.-M. *J. Phys. Chem. B* **1998**, *102*, 9940. (b) Choi, S.-J.; Park, S.-M. *Bull. Korean Chem. Soc.* **2002**, *23*, 699. (c) Amatore, C.; Savenat, J. M.; Tessier, D. *J. Electroanal. Chem.* **1983**, *149*, 39.

(13) (a) Bilewicz, R.; Osteryoung, R. A.; Osteryoung, J. *Anal. Chem.* **1986**, *58*, 2761. (b) Bilewicz, R.; Wikiel, K.; Osteryoung, R.; Osteryoung, J. *Anal. Chem.* **1989**, *61*, 965. (c) He, P. *Anal. Chem.* **1995**, *67*, 986. (d) Osteryoung, J. *Acc. Chem. Res.* **1993**, *26*, 77.

(14) (a) Pyun, C.-H.; Park, S.-M. *J. Electrochem. Soc.* **1985**, *132*, 2426. (b) Shim, Y.-B.; Park, S.-M. *J. Electroanal. Chem.* **1997**, *425*, 201. (c) Kim, Y.-O.; Jung, Y. M.; Kim, S. B.; Park, S.-M. *Anal. Chem.* **2004**, *76*, 5238. (d) Krysiñski, P.; Rrzostowstak-Smolska, M. *J. Electroanal. Chem.* **1997**, *424*, 61.

(15) (a) Nicholson, R. S. *Anal. Chem.* **1965**, *37*, 1351. (b) Chapter 6 of ref 1.

(16) Barsoukov, E., Macdonald, J. R., Eds. *Impedance Spectroscopy: Theory, Experiment, and Applications*, 2nd ed.; Wiley-Interscience: Hoboken, NJ, 2005.

(17) Schmickler, W. *Interfacial Electrochemistry*; Oxford: New York, 1996; pp 45−51.

(18) Bockris, J. O'M.; Reddy, A. K. N.; Gamboa-Aldeco, M. *Modern Electrochemistry*; Kluwer Academic/Plenum Publishers: New York, 2000; Vol. 2A, p 862.

(19) Jurczakowski, R.; Lasia, A. *Anal. Chem.* **2004**, *76*, 5033.

(20) (a) Delahay, P. *J. Am. Chem. Soc.* **1953**, *75*, 5. 1430. (b) See Chapter 5 of ref 1.

(21) Krysiński, P.; Brzostowska-Smaolska *J. Electroanal. Chem.* **1997**, *424*, 61.

(22) (a) Wang, M.; Wang, L.; Wang, G.; Ji, X.; Bai, Y.; Li, T.; Gong, S.; Li, J. *Biosens. Bioelectron.* **2004**, *19*, 575. (b) Darain, F.; Park, D.-S.; Park, J.-S.; Shim, Y.-B. *Biosens. Bioelectron.* **2004**, *19*, 1245. (c) Yang, L.; Lee, Y.; Erf, G. F. *Anal. Chem.* **2004**, *76*, 1107. (d) Zayats, M.; Raitman, O. A.; Chegel, V. I.; Kharitonov, A. B.; Willner, I. *Anal. Chem.* **2002**, *74*, 4763. (e) Lee, T.-Y.; Shim, Y.-B. *Anal. Chem.* **2001**, *73*, 5629.